In-Plane 2H-1T′ $MoTe_2$ Homojunctions Synthesized by Flux-Controlled Phase Engineering

*Youngdong Yoo, Zachary P. DeGregorio, Yang Su, Steven J. Koester, and James E. Johns**

The fabrication of in-plane 2H-1T′ $MoTe_2$ homojunctions by the flux-controlled, phase-engineering of few-layer $MoTe_2$ from Mo nanoislands is reported. The phase of few-layer $MoTe_2$ is controlled by simply changing Te atomic flux controlled by the temperature of the reaction vessel. Few-layer 2H $MoTe_2$ is formed with high Te flux, while few-layer 1T′ $MoTe_2$ is obtained with low Te flux. With medium flux, few-layer in-plane 2H-1T′ $MoTe_2$ homojunctions are synthesized. As-synthesized $MoTe_2$ is characterized by Raman spectroscopy and X-ray photoelectron spectroscopy. Kelvin probe force microscopy and Raman mapping confirm that in-plane 2H-1T′ $MoTe_2$ homojunctions have abrupt interfaces between 2H and 1T′ $MoTe_2$ domains, possessing a potential difference of about 100 mV. It is further shown that this method can be extended to create patterned metal–semiconductor junctions in $MoTe_2$ in a two-step lithographic synthesis. The flux-controlled phase engineering method could be utilized for the large-scale controlled fabrication of 2D metal–semiconductor junctions for next-generation electronic and optoelectronic devices.

Atomically thin transition metal dichalcogenides (TMDCs) have been intensively studied as emerging 2D materials for flexible electronics and optoelectronics due to their unique properties such as a sizable band gap which is absent in the most studied 2D material, graphene.[1–11] Layered TMDCs with the formula MX_2 (M: Mo, W, Nb, or Ta and X: S, Se, or Te) have a wide variety of electronic properties ranging from metallic to semimetallic and semiconducting depending on their atomic combination.[1–4] More interestingly, the electronic properties of TMDCs are further enriched by their polymorphism varying in stacking orders and coordination geometry of the metal center. For Mo- and W-based TMDCs, the 2H phase with trigonal prismatic coordination is semiconducting, while the 1T phase with octahedral coordination is metallic.[1–4] However, tailoring the electronic properties of TMDCs through phase engineering is challenging due to the metastability of 1T TMDCs and the significant free energy difference between 2H and 1T TMDCs.[12–14]

$MoTe_2$ has attracted much interest due to its novel properties such as its narrow bandgap of 0.9–1.1 eV, close to that of silicon (1.1 eV) in the 2H polymorph and its strong spin–orbit coupling.[15–18] These properties are essential for optoelectronic devices operating in the near-infrared range and efficient spintronic and valleytronic devices. One of the most important features of $MoTe_2$ is its phase tunability, originating from a very small free energy difference (40 meV per unit cell) between 2H and 1T′ $MoTe_2$.[13,19,20] Although semiconducting 2H $MoTe_2$ is the most thermodynamically favorable phase, semimetallic 1T′ $MoTe_2$ that is distorted from 1T $MoTe_2$ through a Peierls distortion can also be favored under certain conditions.[21,22] It has been reported that 2H $MoTe_2$ transforms into 1T′ $MoTe_2$ under applied tensile strain or under Te deficiency induced by laser illumination.[19,20] If the phase of $MoTe_2$ could be controlled by simply adjusting the reaction conditions, it would enable the mass production of phase-patterned $MoTe_2$ for device fabrication.

Electronic and optoelectronic applications of 2D TMDCs require semiconductor–semiconductor junctions to build in functionality (e.g., p-n junctions, diodes, etc.) and metal–semiconductor contacts to inject charges. For 2D semiconductor–semiconductor junctions, in-plane semiconducting TMDC heterostructures such as MoS_2/WS_2 and MoS_2/WSe_2 have been synthesized to obtain an abrupt change in electronic and optical properties across atomically sharp junctions.[23–27] For metal–semiconductor junctions, edge contacts have been formed in 2D materials to increase transistor "on" currents and also increase effective charge mobility compared to top metal contacts.[28,29] Furthermore, when the metal and semiconducting materials are two phases of the same material, the barrier to charge injection can be quite low resulting in ideal, minimally resistive Ohmic contacts.[12,19] Metal–semiconductor homojunctions in $MoTe_2$ have been previously fabricated via applied strain or laser illumination,[19,20] but to the best of our knowledge, no one has reported a direct synthetic approach for creating these important metal–semiconductor homojunctions in any 2D material.

Here we report on the fabrication of in-plane 2H-1T′ $MoTe_2$ homojunctions by the flux-controlled, phase-engineering of

Dr. Y. Yoo, Z. P. DeGregorio, Prof. J. E. Johns
Department of Chemistry
University of Minnesota
Minneapolis, MN 55455, USA
E-mail: jjohns@umn.edu
Y. Su, Prof. S. J. Koester
Department of Electrical and Computer Engineering
University of Minnesota
Minneapolis, MN 55455, USA

DOI: 10.1002/adma.201605461

few-layer $MoTe_2$ from Mo nanoislands. We control the phase of few-layer $MoTe_2$ by simply changing Te atomic flux controlled by the temperature of the reaction vessel. Few-layer 2H $MoTe_2$ is formed with high Te flux, while few-layer 1T′ $MoTe_2$ is obtained with low Te flux. With medium flux, we synthesize few-layer in-plane 2H-1T′ $MoTe_2$ homojunctions. As-synthesized $MoTe_2$ is characterized by Raman spectroscopy and X-ray photoelectron spectroscopy (XPS). Kelvin probe force microscopy (KPFM) and Raman mapping confirm that in-plane 2H-1T′ $MoTe_2$ homojunctions have abrupt interfaces between 2H and 1T′ $MoTe_2$ domains, possessing a potential difference of about 100 mV. In addition, we fabricate few-layer 2H-1T′ $MoTe_2$ patterns using our phase-selective synthetic strategy. Our flux-controlled phase engineering method could be utilized for the large-scale controlled fabrication of 2D metal–semiconductor junctions for next-generation electronic and optoelectronic devices.

We synthesize in-plane 2H-1T′ $MoTe_2$ homojunctions from Mo nanoislands in a horizontal hot-wall single-zone furnace. Our synthetic strategy is illustrated in **Figure 1**a. Mo nanoislands are deposited on SiO_2/Si substrates through e-beam evaporation. A contact-mode atomic force microscopy (AFM) image and the height line profile show that the Mo nanoislands have heights of about 1–3 nm and widths of about a few hundred nanometers (Figure S1a,c, Supporting Information). The morphology of the Mo nanoislands is similar to that of conventional transition metal nanoislands formed by e-beam evaporation.[30] The Mo nanoislands on SiO_2/Si substrates are placed face-down on the alumina boat containing lump Te, followed by annealing at 585 °C in Ar/H_2 (5 sccm/5 sccm) environment. Detailed reaction conditions are giving in the Supporting Information. After the reaction, we obtain continuous films possessing uniform surfaces possessing a root-mean-square (RMS) roughness of about 0.88 nm as shown in an AFM image and the height line profile (Figure S1b,d, Supporting Information). Considering that the RMS roughness of the underlying SiO_2/Si substrates is about 0.5–1 nm, we believe the surface of as-synthesized films is quite smooth. The thickness of the film was measured to be about 3.5 nm (Figure S2, Supporting Information), which is consistent with the thickness of five layers of $MoTe_2$.[31,32]

In-plane 2H-1T′ $MoTe_2$ homojunctions are synthesized at 585 °C, while few-layer 2H and 1T′ $MoTe_2$ were formed at 635 and 535 °C respectively. Optical images of 2H (Figure 1b), in-plane 2H-1T′ (Figure 1c), and 1T′ $MoTe_2$ (Figure 1d) few layers show that the $MoTe_2$ has high uniformity and there is a sharp optical contrast between 1T′ and 2H $MoTe_2$ domains (Figure 1b–d).

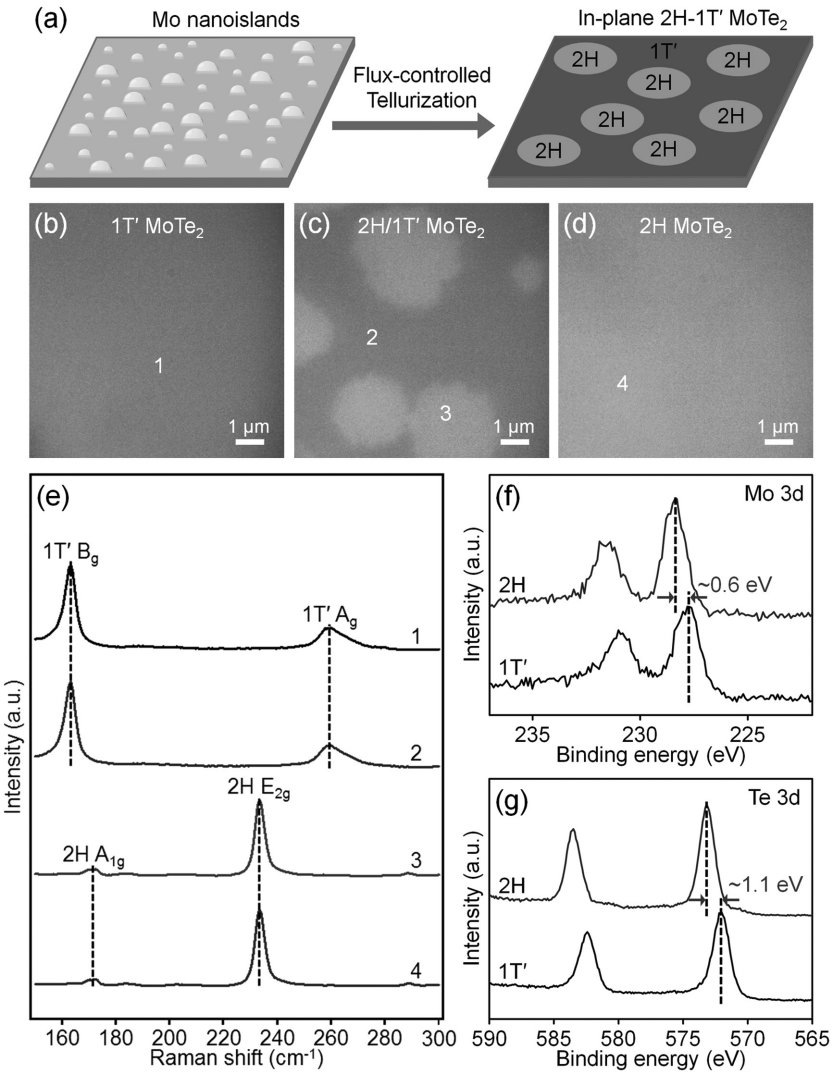

Figure 1. Growth of in-plane 2H-1T′ $MoTe_2$ homojunctions from Mo nanoislands. a) Schematic illustration showing the growth process. b–d) Optical image of few-layer 2H, in-plane 2H-1T′, and 1T′ $MoTe_2$ synthesized at 635, 585, and 535 °C, respectively. e) Raman spectra taken from the points marked by 1–4 in (b)–(d). f) High-resolution XPS spectra showing Mo 3d peaks of few-layer 2H and 1T′ $MoTe_2$. g) High-resolution XPS spectra showing Te 3d peaks of few-layer 2H and 1T′ $MoTe_2$. The Mo 3d and Te 3d peaks of few-layer 1T′ $MoTe_2$ are downshifted by ≈0.6 and ≈1.1 eV, respectively, compared to those of few-layer 2H $MoTe_2$.

The optical contrast is due to the change in visible absorption spectrum of 1T′ and 2H $MoTe_2$.[15,21] Raman spectra taken from the points marked by 1–4 in Figure 1b–d clearly show that 1T′ and 2H $MoTe_2$ domains exhibit phase-specific characteristic Raman peaks, which are the B_g (163.0 cm^{-1}) and A_g (260.1 cm^{-1}) modes for 1T′ $MoTe_2$ and A_{1g} (170.9 cm^{-1}) and E_{2g} (233.5 cm^{-1}) modes for 2H $MoTe_2$, respectively (Figure 1e).[15,33] The crystal structures of as-synthesized few-layer 2H and 1T′ $MoTe_2$ were confirmed by X-ray diffraction (XRD) (Figure S3, Supporting Information).

In order to analyze the elemental composition and the chemical states of few-layer $MoTe_2$, we performed XPS measurements on few-layer 2H and 1T′ $MoTe_2$ formed at 635 and 535 °C, respectively. The XPS survey spectrum confirms the presence of

Mo and Te originating from as-synthesized 2H and 1T′ $MoTe_2$. Adventitious C and O signals are present originating from contamination arising from atmospheric transfer of the material and were used to calibrate the electron binding energies (Figure S4, Supporting Information). The high-resolution XPS peaks for 2H $MoTe_2$ were observed at 228.4 eV (Mo $3d_{5/2}$), 231.5 eV (Mo $3d_{3/2}$), 573.1 eV (Te $3d_{5/2}$), and 583.5 eV (Te $3d_{3/2}$) eV, and those for 1T′ $MoTe_2$ were observed at 227.8 eV (Mo $3d_{5/2}$), 230.9 eV (Mo $3d_{3/2}$), 572.0 eV (Te $3d_{5/2}$), and 582.4 eV (Te $3d_{3/2}$) eV for 1T′ $MoTe_2$, respectively (Figure 1f,g). It has been previously reported that the 1T′ $MoTe_2$ peaks are downshifted by about 0.4–0.6 eV compared to 2H $MoTe_2$.[19,31,32] Interestingly, we observe that the Te 3d peaks are downshifted by about 1.1 eV while the Mo 3d peaks are downshifted by about 0.6 eV in our few-layer 1T′ $MoTe_2$. We attribute the further downshift of Te 3d peaks to Te deficiency in few-layer 1T′ $MoTe_2$. It has been known that chalcogen deficiency in TMDCs decreases the binding energy of the chalcogen while maintaining the binding energy of the transition metal approximately the same.[34] The Te/Mo atomic ratio of our few-layer $MoTe_2$ was quantified by comparing the area ratio of Mo 3d-to-Te 3d peaks of 2H $MoTe_2$ with that of 1T′ $MoTe_2$. When the value of the Te/Mo atomic ratio of 2H $MoTe_2$ is normalized to 2.00, Te/Mo atomic ratio of 1T′ $MoTe_2$ is calculated to be about 1.86.

Based on the Te deficiency of $MoTe_2$ in our few-layer 1T′ $MoTe_2$, we hypothesize that the flux of Te determines the phase of few-layer $MoTe_2$ consistent with the reported crystal growth.[21,35] There are two variables in the experiments presented in Figure 1, which are the substrate temperature and the Te flux. In order to exclude the influence of the substrate temperature on reactions, we performed a series of reactions using the experimental configuration shown in **Figure 2**a. In order to control the Te flux independently, we placed Te lump at four different positions of A (635 °C), B (585 °C), C (535 °C), and D (485 °C), and we maintained the substrate temperature at 635 °C for all reactions. The vapor pressures of Te are calculated to be about 10.9, 4.5, 1.7, and 0.5 Torr for 635, 585, 535, and 485 °C, respectively.[36] Since flux, defined as the number of deposited atoms per unit time and unit area, is proportional to the vapor pressure, the Te flux at 635 °C is estimated to be about 20 times higher than that at 485 °C. Stokes and anti-Stokes Raman spectra show clearly that the sample A (Te: 635 °C) exhibits characteristic Raman peaks of 2H $MoTe_2$ while the sample C (Te: 535 °C) shows characteristic Raman peaks of 1T′ $MoTe_2$ (Figure 2b). Interestingly, the sample B (Te: 585 °C) shows both Raman peaks of 2H and 1T′ $MoTe_2$ (Figure 2b), indicating the sample is composed of mixed 2H-1T′ $MoTe_2$. The sample D (Te: 485 °C) exhibits shifted Raman peaks of 1T′ $MoTe_2$, which are attributed to the severe Te deficiency in the 1T′ $MoTe_2$. Additional details of our Raman measurements including the fitted peak shape are shown in Figure S5 (Supporting Information).

We propose that our synthesis is controlled by thermodynamics because the Mo nanoislands were annealed in a Te environment for a sufficient period of time to reach thermodynamic equilibrium, and that the changes in phase are driven by the chemical potential of the Te. Density functional theory (DFT) calculations have predicted that the 2H $MoTe_2$ is thermodynamically the most stable in stoichiometric $MoTe_2$, while

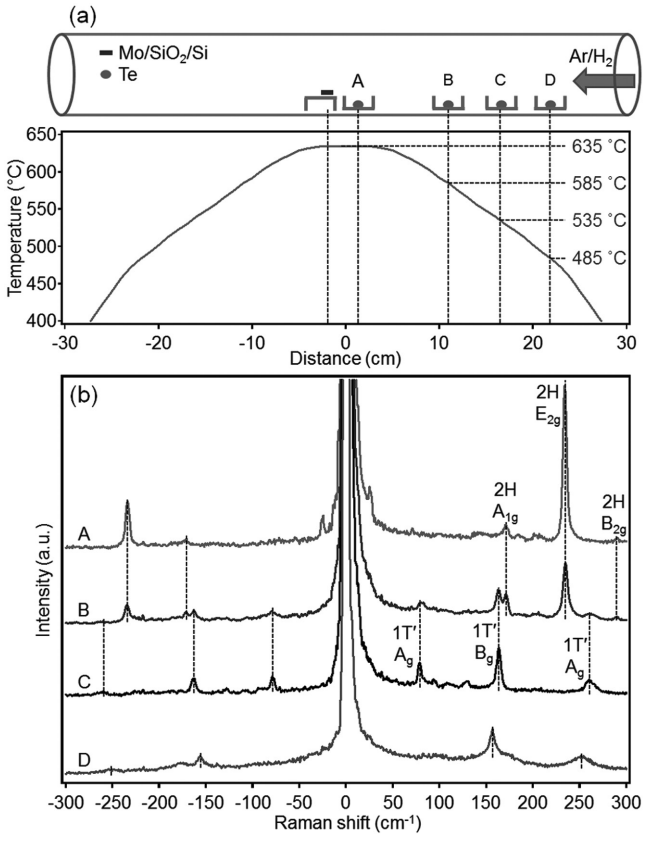

Figure 2. Flux-controlled phase engineering of few-layer $MoTe_2$. a) Schematic illustration showing the experimental setup for flux-controlled reactions and the temperature profiles of the furnace heated at 635 °C. Te lump was placed at positions of A (635 °C), B (585 °C), C (535 °C), and D (485 °C) for the syntheses of few-layer 2H, mixed 2H-1T′, 1T′, and defective 1T′ $MoTe_2$, respectively. The temperature of Mo nanoislands on SiO_2/Si substrates was kept at 635 °C for all experiments. b) Stokes and anti-Stokes Raman spectra of few-layer 2H, mixed 2H-1T′, 1T′, and defective 1T′ $MoTe_2$ synthesized at Te temperatures of 635, 585, 535, and 485 °C, respectively.

the 1T′ $MoTe_2$ gets more stable as the Te vacancy concentration increases.[19] We not only demonstrate experimentally that the phase of $MoTe_2$ is determined thermodynamically by the Te vacancy concentration, but also provide quantitative values of vapor pressures which are optimum for the growth of 2H, mixed 2H-1T′, and 1T′ $MoTe_2$.

The in-plane 2H-1T′ $MoTe_2$ homojunctions are characterized using Raman mapping and KPFM. An optical image of the 2H-1T′ $MoTe_2$ used for Raman mapping shows a clear optical contrast between 2H and 1T′ $MoTe_2$ domains (**Figure 3**a). Raman spectra indicate that the inner circular area and the outer area are composed of 2H and 1T′ $MoTe_2$, respectively (Figure 3b). Raman maps of 2H $MoTe_2$ E_{2g} and 1T′ $MoTe_2$ B_g clearly show that there are abrupt junctions between 2H and 1T′ $MoTe_2$ domains (Figure 3c,d). A KPFM image and the potential line profiles confirm a sharp 100 mV potential difference between 2H and 1T′ $MoTe_2$ domains (Figure 3e,g). The AFM height image and the height line profiles show that there is no significant change in heights of in-plane 2H-1T′ $MoTe_2$ junctions (Figure 3f,h). KPFM measures the contact potential

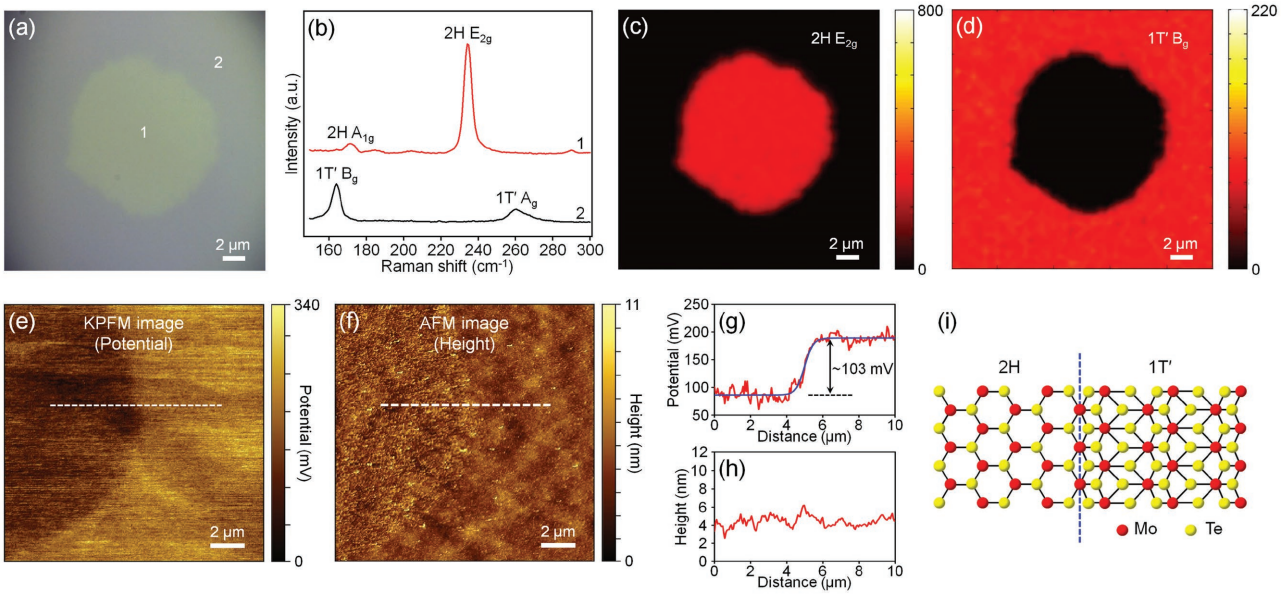

Figure 3. Raman mapping and KPFM study of in-plane 2H-1T′ $MoTe_2$ homojunctions. a) Optical image of in-plane 2H-1T′ $MoTe_2$ homojunctions. b) Raman spectra taken from the points marked by 1 and 2 in (a). c) Raman intensity map of the E_{2g} mode of 2H $MoTe_2$. d) Raman intensity map of the B_g mode of 1T′ $MoTe_2$. e) KPFM potential image of the in-plane 2H-1T′ $MoTe_2$ homojuntions. f) AFM height image of the in-plane 2H-1T′ $MoTe_2$ homojuntions. g) Potential line profiles along the dotted white line of (e). h) Height line profiles along the dotted white line of (f). i) Atomic model of an in-plane junction between 2H and 1T′ $MoTe_2$.

difference (CPD) between the tip and the material.[37] The measured CPDs on 2H and 1T′ $MoTe_2$ are $[\Phi(\text{tip}) - \Phi(\text{2H } MoTe_2)]/e$ and $[\Phi(\text{tip}) - \Phi(\text{1T′ } MoTe_2)]/e$, where Φ(tip), Φ(2H $MoTe_2$), and Φ(1T′ $MoTe_2$) are the work functions for the tip, 2H $MoTe_2$, and 1T′ $MoTe_2$, respectively. Thus, the work function difference between the 2H and 1T′ $MoTe_2$ domains, Φ(2H $MoTe_2$) – Φ(1T′ $MoTe_2$), is simply calculated to be about 100 meV. We believe that the work function difference could be attributed to not only the Te deficiency in 1T′ $MoTe_2$ but also the electronic structure difference between 2H and 1T′ $MoTe_2$. An atomic model of in-plane 2H-1T′ $MoTe_2$ junctions is illustrated in Figure 3i.

Using our phase-selective synthetic strategy, we also fabricated few-layer 2H-1T′ $MoTe_2$ patterns. The fabrication procedure is illustrated in Figure S6 (Supporting Information). As-synthesized few-layer 1T′ $MoTe_2$ is masked by conventional e-beam lithography, and the unmasked few-layer 1T′ $MoTe_2$ is replaced by Mo nanoislands through etching and e-beam evaporation followed by liftoff. This results in patterned regions of 1T′ $MoTe_2$ and Mo nanoislands, which are subsequently annealed with high Te flux to obtain few-layer 2H-1T′ $MoTe_2$ patterns. It is worth noting that the phase of few-layer 1T′ $MoTe_2$ is conserved without phase change or decomposition during annealing with high Te flux (Figure S7, Supporting Information), which is essential for our patterning method. We believe that Te atoms cannot be effectively incorporated into the lattices of as-synthesized few-layer 1T′ $MoTe_2$ under our high Te flux conditions. In essence, once the $MoTe_2$ has been formed in a specific phase, it becomes kinetically trapped in that phase under our reaction conditions. The 2H-1T′ $MoTe_2$ pattern shows a sharp optical contrast between the inner and outer domains (**Figure 4**a). Raman measurements and mapping confirm that the inner and outer domains of the pattern are comprised of 2H and 1T′ $MoTe_2$, respectively, as well as that the pattern has abrupt interfaces between 2H and 1T′ $MoTe_2$ domains (Figure 4b–d).

In conclusion, we demonstrate that the phase of few-layer $MoTe_2$ can be selected by the flux-controlled tellurization of Mo nanoislands. We synthesize for the first time few-layer in-plane 2H-1T′ $MoTe_2$ homojunctions at optimum Te flux conditions. Few-layer 1T′ $MoTe_2$ is obtained with low Te flux, while few-layer 2H $MoTe_2$ is formed with high Te flux. With very low Te

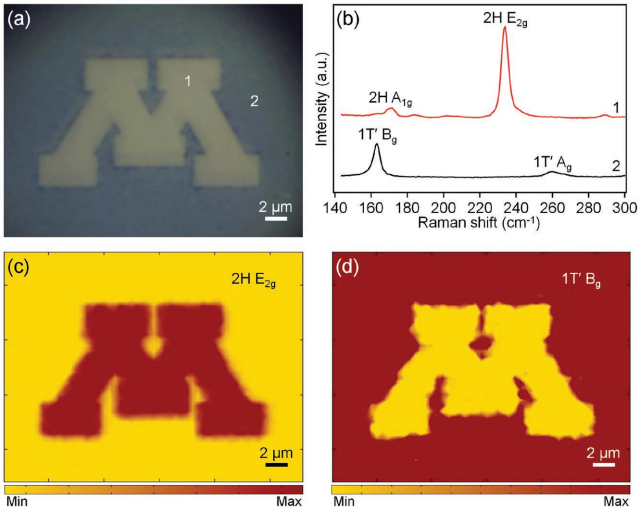

Figure 4. Fabrication of few-layer 2H-1T′ $MoTe_2$ patterns. a) Optical image of 2H-1T′ $MoTe_2$ patterns. b) Raman spectra taken from the points marked by 1 and 2 in (a). c) Raman intensity map of the E_{2g} mode of 2H $MoTe_2$. d) Raman intensity map of the B_g mode of 1T′ $MoTe_2$.

flux, defective 1T′ $MoTe_2$ is synthesized. Raman mapping and KPFM confirm that the junctions of few-layer in-plane 2H-1T′ $MoTe_2$ have a sharp interface possessing a sizable potential difference of 100 meV between 2H and 1T′ $MoTe_2$ domains. Furthermore, we show that our phase-selective $MoTe_2$ synthesis can be utilized for the fabrication of few-layer 2H-1T′ $MoTe_2$ patterns. We believe our flux-controlled synthetic approach developed here opens up the possibility of large-scale direct fabrication of patterned edge-contact 2D material devices.

Supporting Information

Supporting Information is available from the Wiley Online Library or from the author.

Acknowledgements

J.E.J. and Y.Y. acknowledge the donors of the American Chemical Society Petroleum Research Fund (55709-DNI5) for funding and support of this research. S.J.K. and Y.S. were supported by the Defense Threat Reduction Agency Basic Research Award no. HDTRA1-14-1-0042. Parts of this work were carried out in the Characterization Facility, University of Minnesota, which has received capital equipment funding from the National Science Foundation through the MRSEC program under Award Number DMR-1420013.

Received: October 10, 2016
Revised: January 9, 2017
Published online: February 21, 2017

[1] Q. H. Wang, K. Kalantar-Zadeh, A. Kis, J. N. Coleman, M. S. Strano, *Nat. Nanotechnol.* **2012**, *7*, 699.
[2] M. Chhowalla, H. S. Shin, G. Eda, L.-J. Li, K. P. Loh, H. Zhang, *Nat. Chem.* **2013**, *5*, 263.
[3] R. Lv, J. A. Robinson, R. E. Schaak, D. Sun, Y. Sun, T. E. Mallouk, M. Terrones, *Acc. Chem. Res.* **2015**, *48*, 56.
[4] S. Z. Butler, S. M. Hollen, L. Cao, Y. Cui, J. A. Gupta, H. R. Gutierrez, T. F. Heinz, S. S. Hong, J. Huang, A. F. Ismach, E. Johnston-Halperin, M. Kuno, V. V. Plashnitsa, R. D. Robinson, R. S. Ruoff, S. Salahuddin, J. Shan, L. Shi, M. G. Spencer, M. Terrones, W. Windl, J. E. Goldberger, *ACS Nano* **2013**, *7*, 2898.
[5] K. F. Mak, C. Lee, J. Hone, J. Shan, T. F. Heinz, *Phys. Rev. Lett.* **2010**, *105*, 136805.
[6] D. Xiao, G. B. Liu, W. X. Feng, X. D. Xu, W. Yao, *Phys. Rev. Lett.* **2012**, *108*, 196802.
[7] Y. H. Lee, X. Q. Zhang, W. J. Zhang, M. T. Chang, C. T. Lin, K. D. Chang, Y. C. Yu, J. T. W. Wang, C. S. Chang, L. J. Li, T. W. Lin, *Adv. Mater.* **2012**, *24*, 2320.
[8] J. Mann, Q. Ma, P. M. Odenthal, M. Isarraraz, D. Le, E. Preciado, D. Barroso, K. Yamaguchi, G. von Son Palacio, A. Nguyen, T. Tran, M. Wurch, A. Nguyen, V. Klee, S. Bobek, D. Sun, T. F. Heinz, T. S. Rahman, R. Kawakami, L. Bartels, *Adv. Mater.* **2014**, *26*, 1399.
[9] C. Ko, Y. Lee, Y. Chen, J. Suh, D. Fu, A. Suslu, S. Lee, J. D. Clarkson, H. S. Choe, S. Tongay, R. Ramesh, J. Wu, *Adv. Mater.* **2016**, *28*, 2923.
[10] E. Kim, C. Ko, K. Kim, Y. Chen, J. Suh, S.-G. Ryu, K. Wu, X. Meng, A. Suslu, S. Tongay, J. Wu, C. P. Grigoropoulos, *Adv. Mater.* **2016**, *28*, 341.
[11] Y. He, A. Sobhani, S. Lei, Z. Zhang, Y. Gong, Z. Jin, W. Zhou, Y. Yang, Y. Zhang, X. Wang, B. Yakobson, R. Vajtai, N. J. Halas, B. Li, E. Xie, P. Ajayan, *Adv. Mater.* **2016**, *28*, 5126.
[12] R. Kappera, D. Voiry, S. E. Yalcin, B. Branch, G. Gupta, A. D. Mohite, M. Chhowalla, *Nat. Mater.* **2014**, *13*, 1128.
[13] K. A. Duerloo, Y. Li, E. J. Reed, *Nat. Commun.* **2014**, *5*, 4214.
[14] Q. Tang, D.-E. Jiang, *Chem. Mater.* **2015**, *27*, 3743.
[15] C. Ruppert, O. B. Aslan, T. F. Heinz, *Nano Lett.* **2014**, *14*, 6231.
[16] A. Arora, R. Schmidt, R. Schneider, M. R. Molas, I. Breslavetz, M. Potemski, R. Bratschitsch, *Nano Lett.* **2016**, *16*, 3624.
[17] I. G. Lezama, A. Arora, A. Ubaldini, C. Barreteau, E. Giannini, M. Potemski, A. F. Morpurgo, *Nano Lett.* **2015**, *15*, 2336.
[18] Q. Zhang, S. A. Yang, W. Mi, Y. Cheng, U. Schwingenschlögl, *Adv. Mater.* **2016**, *28*, 959.
[19] S. Cho, S. Kim, J. H. Kim, J. Zhao, J. Seok, D. H. Keum, J. Baik, D.-H. Choe, K. J. Chang, K. Suenaga, S. W. Kim, Y. H. Lee, H. Yang, *Science* **2015**, *349*, 625.
[20] S. Song, D. H. Keum, S. Cho, D. Perello, Y. Kim, Y. H. Lee, *Nano Lett.* **2016**, *16*, 188.
[21] D. H. Keum, S. Cho, J. H. Kim, D.-H. Choe, H.-J. Sung, M. Kan, H. Kang, J.-Y. Hwang, S. W. Kim, H. Yang, K. J. Chang, Y. H. Lee, *Nat. Phys.* **2015**, *11*, 482.
[22] L. Huang, T. M. McCormick, M. Ochi, Z. Zhao, M.-T. Suzuki, R. Arita, Y. Wu, D. Mou, H. Cao, J. Yan, N. Trivedi, A. Kaminski, *Nat. Mater.* **2016**, *15*, 1155.
[23] Y. J. Gong, J. H. Lin, X. L. Wang, G. Shi, S. D. Lei, Z. Lin, X. L. Zou, G. L. Ye, R. Vajtai, B. I. Yakobson, H. Terrones, M. Terrones, B. K. Tay, J. Lou, S. T. Pantelides, Z. Liu, W. Zhou, P. M. Ajayan, *Nat. Mater.* **2014**, *13*, 1135.
[24] M. Y. Li, Y. Shi, C. C. Cheng, L. S. Lu, Y. C. Lin, H. L. Tang, M. L. Tsai, C. W. Chu, K. H. Wei, J. H. He, W. H. Chang, K. Suenaga, L. J. Li, *Science* **2015**, *349*, 524.
[25] H. Heo, J. H. Sung, G. Jin, J.-H. Ahn, K. Kim, M.-J. Lee, S. Cha, H. Choi, M.-H. Jo, *Adv. Mater.* **2015**, *27*, 3803.
[26] Y. Yoo, Z. P. Degregorio, J. E. Johns, *J. Am. Chem. Soc.* **2015**, *137*, 14281.
[27] K. Chen, X. Wan, W. Xie, J. Wen, Z. Kang, X. Zeng, H. Chen, J. Xu, *Adv. Mater.* **2015**, *27*, 6431.
[28] M. H. D. Guimarães, H. Gao, Y. Han, K. Kang, S. Xie, C.-J. Kim, D. A. Muller, D. C. Ralph, J. Park, *ACS Nano* **2016**, *10*, 6392.
[29] A. Allain, J. Kang, K. Banerjee, A. Kis, *Nat. Mater.* **2015**, *14*, 1195.
[30] G. Seguini, J. L. Curi, S. Spiga, G. Tallarida, C. Wiemer, M. Perego, *Nanotechnology* **2014**, *25*, 495603.
[31] L. Zhou, K. Xu, A. Zubair, A. D. Liao, W. Fang, F. Ouyang, Y.-H. Lee, K. Ueno, R. Saito, T. Palacios, J. Kong, M. S. Dresselhaus, *J. Am. Chem. Soc.* **2015**, *137*, 11892.
[32] C. H. Naylor, W. M. Parkin, J. Ping, Z. Gao, Y. R. Zhou, Y. Kim, F. Streller, R. W. Carpick, A. M. Rappe, M. Drndic, J. M. Kikkawa, A. T. Johnson, *Nano Lett.* **2016**, *16*, 4297.
[33] S.-Y. Chen, T. Goldstein, D. Venkataraman, A. Ramasubramaniam, J. Yan, *Nano Lett.* **2016**, *16*, 5852.
[34] H. Li, C. Tsai, A. L. Koh, L. Cai, A. W. Contryman, A. H. Fragapane, J. Zhao, H. S. Han, H. C. Manoharan, F. Abild-Pedersen, J. K. Norskov, X. Zheng, *Nat. Mater.* **2016**, *15*, 48.
[35] L. Zhou, A. Zubair, Z. Wang, X. Zhang, F. Ouyang, K. Xu, W. Fang, K. Ueno, J. Li, T. Palacios, J. Kong, M. S. Dresselhaus, *Adv. Mater.* **2016**, *28*, 9526.
[36] L. S. Brooks, *J. Am. Chem. Soc.* **1952**, *74*, 227.
[37] J. L. Neff, P. Rahe, *Phys. Rev. B* **2015**, *91*, 085424.

